Nuclear Materials and Energy 33 (2022) 101266

Contents lists available at ScienceDirect

Nuclear Materials and Energy

journal homepage: www.elsevier.com/locate/nme

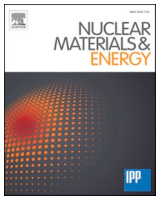

Influence of surface morphology on erosion of plasma-facing components in H-mode plasmas of ASDEX Upgrade

A. Lahtinen [a], A. Hakola [a,*], J. Likonen [a], M. Balden [b], K. Krieger [b], S. Gouasmia [c], I. Bogdanovic Radovic [c], G. Provatas [c], M. Kelemen [d], S. Markelj [d], M. Pedroni [e], A. Uccello [e], E. Vassallo [e], D. Dellasega [f], M. Passoni [f], ASDEX Upgrade Team[1], EUROfusion MST1 Team[2]

[a] VTT, P. O. Box 1000, 02044 VTT, Finland
[b] Max-Planck-Institut für Plasmaphysik, Boltzmannstr. 2, 85748 Garching, Germany
[c] Ruder Boskovic Institute, Bijenicka 54, 10000 Zagreb, Croatia
[d] Jozef Stefan Institute, Jamova cesta 39, 1000 Ljubljana, Slovenia
[e] Istituto per la Scienza e Tecnologia dei Plasmi CNR, Milan, Italy
[f] Politecnico di Milano, Department of Energy, Milan, Italy

ARTICLE INFO

Keywords:
Erosion
Material migration
ASDEX Upgrade
H-mode
Marker samples

ABSTRACT

Net erosion of plasma-facing materials was investigated at the low-field-side (outer) strike-point area of the ASDEX Upgrade (AUG) divertor during H-mode discharges with small and frequent ELMs. To this end, Au and Mo marker samples with different surface morphologies and geometries were exposed to plasmas using the DIM-II divertor manipulator. The results were compared to existing erosion and deposition patterns from various L- and H-mode experiments, in the latter case the main difference was the size and frequency of the ELMs.

We noticed that increasing surface roughness reduces net erosion but less than what is the case in L-mode. On the other hand, net-erosion rates in H-mode are generally 2–5 times higher than the corresponding L-mode values, in addition to which exposure in H-mode conditions results in strong local variations in the poloidal and toroidal erosion/deposition profiles. The latter observation we associate with the large migration length, on the order of several cm, of the eroded material, resulting in strong competition between erosion and re-deposition processes especially at poloidal distances $>$ 50 mm from the strike point. Considerable net erosion was measured throughout the analysed poloidal region unlike in L-mode where the main erosion peak occurs in the vicinity of the strike point. We attribute this qualitative difference to the slow decay lengths of the plasma flux and electron temperature in the applied H-mode scenario.

Both erosion and deposition require detailed analyses at the microscopic scale and the deposition patterns may be drastically different for heavy and light impurities. Generally, the rougher the surface the more material will accumulate on locally shadowed regions behind protruding surface features. However, rough surfaces also exhibit more non-uniformities in the quality or even integrity of marker coatings produced on them, thus complicating the analyses of the experimental data.

We conclude that local plasma parameters have a huge impact on the PFC erosion rates and, besides incident plasma flux, surface morphology and its temporal evolution have to be taken into account for quantitative estimates of erosion rates and PFC lifetime under reactor-relevant conditions.

Introduction

The plasma-facing components (PFCs) of future fusion power plants will be subjected to large power and particle fluxes during the operational periods of the reactor. This may compromise the lifetime of the PFCs in the most heavily exposed areas, thus calling for detailed investigations on the behaviour of potential PFC materials in a variety of plasma scenarios. Tungsten (W) is one of the main candidate materials

* Corresponding author at: VTT, P. O. Box 1000, 02044 VTT, Finland.
E-mail address: antti.hakola@vtt.fi (A. Hakola).
[1] See author list of U. Stroth et al. 2022 Nucl. Fusion 62 042006
[2] See author list of B. Labit et al. 2019 Nucl. Fusion 59 086020

https://doi.org/10.1016/j.nme.2022.101266
Received 30 June 2022; Received in revised form 8 September 2022; Accepted 29 September 2022
Available online 3 October 2022
2352-1791/© 2022 Published by Elsevier Ltd. This is an open access article under the CC BY-NC-ND license (http://creativecommons.org/licenses/by-nc-nd/4.0/).

for the PFCs, and recently much effort has been put on exposing W-based structures to pre-determined sets of plasma discharges, including off-normal events, in different tokamaks such as ASDEX Upgrade (AUG) [1], DIII-D [2,3], JET [4], and WEST [5].

Surface morphology of W PFCs has been observed to strongly affect their erosion characteristics, in particular the balance between *gross and net erosion* [1]; here, gross erosion denotes the material directly sputtered from the PFC surfaces by plasma bombardment while net erosion takes into account the fraction of eroded particles re-deposited in areas close to their origin. Data collected from *marker samples* at a fixed position in a reactor, either in the *divertor* or in the *main chamber*, indicate that with increasing surface roughness net erosion strongly decreases and may even change into apparent net deposition [1,6–8]. In addition, distinct features created on the surface before the sample exposure show the local nature of erosion and re-deposition patterns: elevated areas manifest enhanced erosion while recessed or shadowed regions are more prone to be dominated by deposition [9].

However, up to now both the experimental and modelling efforts related to W erosion have concentrated on L-mode discharges [10,11], while H-mode plasmas would represent cases more relevant for ITER and DEMO. To cast light into the differences between L- and H-mode discharges, additional experiments have recently been carried out on AUG, by making use of the most attractive features of the device: the full-W plasma environment, the versatile heating capabilities, and the upgraded divertor manipulator (DIM-II) [12], which enables exposing desired samples to well-characterized plasma discharges in one toroidal sector, around the *low-field-side (outer) strike point region* (OSP) of the AUG divertor.

A lesson learnt from the past erosion studies on AUG is that surface roughness cannot be fully described by a single parameter, typically mean arithmetic roughness R_a, but a proper microscopic description of the surface is needed. With this in mind, we have determined the erosion profiles by coupling standard ion-beam analyses to detailed microscopy measurements but have also prepared samples with regular and uniform morphology patterns. All these have helped us in proceeding towards micrometre length scales.

In the following, we will discuss the results obtained from an H-mode experiment on AUG, performed in 2020, with regular and relatively small edge-localized modes (ELMs). The erosion data will be put into perspective by comparing them with the already published [1] profiles in a variety of L-mode discharges as well as in H-mode with large ELMs.

Experimental details

Samples used in the experiments

Two different types of samples were used in the AUG experiment, labelled S-a and S-b, in accordance with the naming scheme introduced in [1]. In all cases, the samples were 33.5 mm long (oriented in the poloidal direction of the AUG divertor), 12 mm wide (in the toroidal direction), and flush-mounted (elevations between + 0.1 mm and − 0.15 mm, did not alter the centre point of the analysed samples) on dedicated target tiles (made of bulk W) of the divertor manipulator DIM-II. As marker materials, molybdenum (Mo) and gold (Au) were used, also to serve as proxies to W due to the full-W coverage of the AUG first wall. Based on earlier results in [10], the absolute erosion values of Au and Mo differ from those of W by a factor of 5–10, whereas the re-deposition patterns of especially Au and W have been noticed to be comparable [10]. Therefore, the ionization properties and, consequently, migration lengths of the eroded particles for the two elements are similar – only the sputtering rates are different.

- *Type S-a*: Fine-grained graphite samples with a Mo marker layer (thickness ~ 300 nm) and Au marker spots (thickness 50–60 nm, lateral dimensions 1 × 1 mm^2 and 5 × 5 mm^2) on top. The graphite substrates were treated such that their mean arithmetic surface roughness was R_a < 0.2 μm. The small spots were used for determining gross erosion while the larger spots were designed for assessing net erosion as discussed in [1,10]. The concept was pioneered in DIII-D with 1-mm and 10-mm diameter W and Mo disks, and re-deposition was noticed to be negligible on the smaller samples [3].
- *Type S-b*: Fine-grained graphite samples with varying morphologies on their surfaces and equipped with an ~ 150 nm thick Mo marker layer. The samples showed three different roughness levels of R_a ~ 0.1 μm, 0.3 μm, and 1 μm.

Fig. 1a shows a schematic illustration of the samples and their locations on the DIM-II target tiles during the actual experiment, around the OSP region. In addition to type S-a and S-b samples, Mo- or rhenium (Re)-coated pieces of fine-grained graphite (R_a < 0.2 μm) had been installed on the target tiles but these are not discussed in this article.

The type S-b samples with roughness levels of R_a ~ 0.1 μm and 0.3 μm were first polished, starting from the same surface state as realized on the S-a samples, after which fluorine-based (using CF_4), radio-frequency (RF) plasma etching was performed at Istituto per la Scienza e Tecnologia dei Plasmi (CNR) in Milan, Italy, to create the desired surface state. The roughest samples (R_a ~ 1 μm), for their part, resulted from glass-bead blasting of the original graphite surface.

The marker coatings on the type S-a samples were realized using arc-discharge sputtering [13] by Oerlikon Surface Solutions in Finland while the type S-b samples were coated by pulsed laser deposition (PLD) in Politecnico di Milano. The most essential PLD parameters were: laser wavelength 1064 nm, laser fluence 2.1 J/cm^2, deposition time 21 min at a base vacuum of 10^{-2} Pa and with a target-substrate distance of 130 mm. This resulted in a uniform coverage of the surface such that the underlying substrate topography could be faithfully preserved. The PLD coatings were characterized both before and after their production using Atomic Force Microscopy (AFM) and Scanning Electron Microscopy (SEM). AFM images of the surface of an R_a ~ 0.3 μm sample before and after its surface treatment can be seen in Fig. 2. Please note that in part (b) the surface may feature high peaks or deep depressions in the micrometre scale but across the entire sample the target value for the (average) R_a was well reached.

Once the coating steps were completed, both type S-a and S-b samples were analysed using SEM-EDX (Energy Dispersive X-ray Spectroscopy, ZEISS Auriga 60 with Bruker Quantax EDX XFlash 430 and WDX XSense) and broad-beam Rutherford Backscattering Spectrometry (RBS) at the Max-Planck-Institut für Plasmaphysik in Garching, Germany. These analyses were repeated after the actual experiment to determine the changes in the thickness and terrain of the marker coatings typically along the poloidal direction (see Fig. 1 for definition). In RBS, 2-MeV $^4He^+$ -beam (size ~ mm^2) was used and the backscattered particles were detected at 165°; fitting of the RBS data was performed using the SIMNRA software [14]. Finally, the samples were transported to Ruđer Bošković Institute in Zagreb, Croatia, and Jožef Stefan Institute in Ljubljana, Slovenia, for detailed RBS and Proton-Induced X-ray Emission (PIXE) measurements of their surfaces, also in the micrometre length scale. The micro-RBS and micro-PIXE were the only tools besides SEM-EDX that provided information on the surface changes of the small 1 × 1 mm^2 marker spots. In the microbeam measurements, protons with an energy of 2 MeV were focused to a ~ 4 × 4 $μm^2$ spot. The analysed sample surface in each run was ~ 750 × 750 $μm^2$. The X-ray spectra were measured by means of a 30-mm^2 active area and 450-μm thick Sirius Series SDD detector, placed at 125°.

Experiments on ASDEX Upgrade

The H-mode experiment discussed here was carried out in deuterium (D) and such that the ELMs would not be too large to result in complete removal of the marker coatings during the first discharge. According to the numbering scheme introduced in [1], it will be referred to as

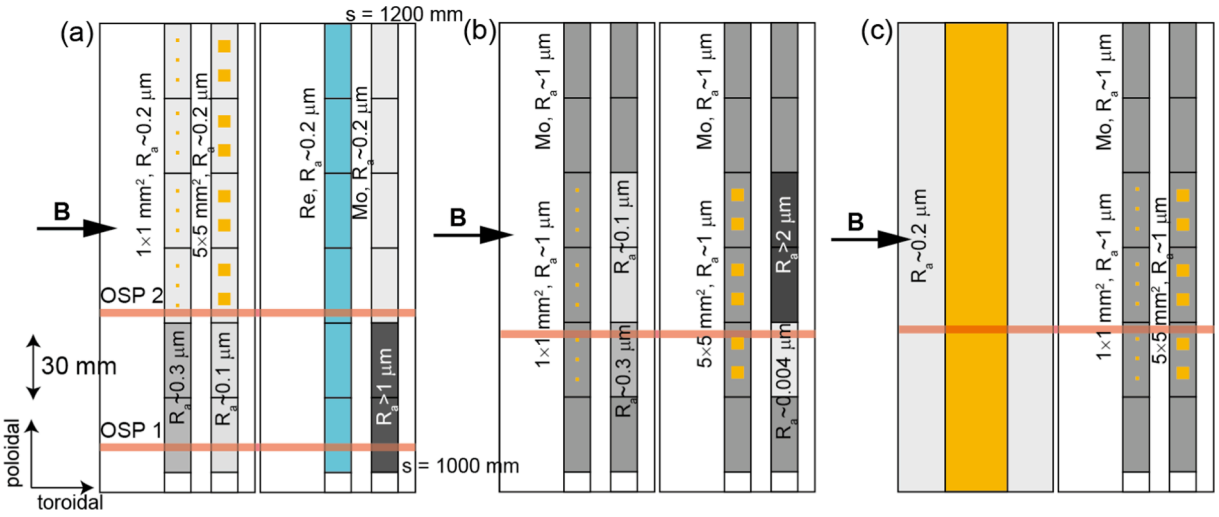

Fig. 1. Schematic illustration of the marker samples mounted on the DIM-II divertor manipulator head for the different H- and L-mode plasma experiments on ASDEX Upgrade. (a) Experiment E3 with Au markers (type S-a) and Mo roughness samples (type S-b); (b) experiment E1b (L-mode) with type S-a and S-b samples; and (c) experiment E2 (H-mode with large type-I ELMs) with type S-a samples as well as a bulk W tile with Au and Mo markers. The strike-point positions are denoted by red horizontal bars, different shades for the grey background colour stand for Mo, yellow for Au, blue for Re, and white for W. (For interpretation of the references to colour in this figure legend, the reader is referred to the web version of this article.)

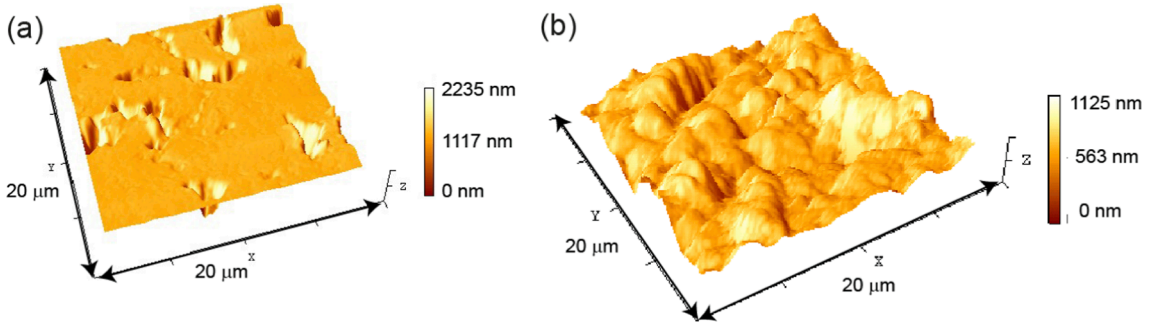

Fig. 2. AFM images of (a) the graphite substrate ($R_a < 0.2$ µm) of type S-b samples before surface treatment and (b) after the plasma-etching step of the same samples with the target value of $R_a \sim 0.3$ µm for the mean surface roughness.

experiment E3. The comparative data is taken from earlier L- and H-mode experiments, called experiments E1b and E2, respectively, and reported in [1].

The experiment E3 consisted of two parts, illustrated by two different OSP positions, marked with OSP1 and OSP2 in Fig. 1a. The two strike points were separated by roughly 60 mm, corresponding to s≈1010 mm (OSP1) and s≈1070 mm (OSP2) for the values of the poloidal *s*-coordinate. At and around OSP1, samples of type S-b were subjected to plasma discharges while in the surroundings of OSP2, type S-a samples (as well as the remaining Re and Mo coatings) had been installed. One should, however, notice that the S-a samples were also exposed to peripheral plasmas during the OSP1 phase while in the subsequent OSP2 phase, the S-b samples ended up in the *private flux region* (PFR) and thereby their topmost parts in a strong net deposition zone as stated in Refs. [15,16].

The main parameters used were toroidal magnetic field $B_t = 2.5$ T, plasma current $I_p = 0.6$ MA, core plasma density $n_e \sim 8.5 \times 10^{19}$ m^{-3}, and auxiliary heating with neutral beam injection (NBI) and electron cyclotron resonance heating (ECRH) at $P_{NBI} = 5.0$ MW and $P_{ECRH} = 4.0$ MW, respectively. Based on Langmuir probe measurements, the peak values for the plasma flux in terms of the ion saturation current were $j_{sat} \sim 1.0$–1.5×10^{23} m^{-2} s^{-1} and for the electron temperature $T_e \sim 20$–25 eV. The profiles for the flux and electron temperature during the OSP1 and OSP2 phases can be seen in Fig. 3. The ELM frequency and associated energy loss per ELM were 125 Hz and 10 kJ, respectively, and the normalized energy loss per ELM was $\Delta W_{ELM}/W_{MHD} \sim 0.011$.

In the OSP1 phase, two consecutive discharges (AUG shots #38069–38070) were applied, corresponding to the overall plasma flat-top time of ~ 6 s, while in the OSP2 phase three discharges (#38071–38073) were carried out and such that the flat-top time was ~ 9 s. An example of the time traces for the key plasma parameters in the two phases can be seen in Fig. 4a and 4b. Fig. 4c, for its part, shows the residence time of the OSP as a function of the poloidal *s*-coordinate, indeed proving that the two strike point regions were well separated from each other.

The experiments E1b and E2 (reported in [1]) had the following specifications:

- *Experiment E1b*: Toroidal magnetic field $B_t = 2.5$ T, plasma current $I_p = 0.8$ MA, core plasma density $n_e \sim 4 \times 10^{19}$ m^{-3}, and auxiliary heating using ECRH only at $P_{ECRH} = 0.7$ MW. The electron temperature at the OSP was $T_e \sim 20$–30 eV and the overall exposure time of the marker samples ~ 28 s, see [10]. Both type S-a and S-b samples were used (see Fig. 1b) but this time the S-a samples had a larger surface roughness of $R_a \sim 1$ µm while the S-b samples exhibited a range of roughnesses ($R_a \sim 0.004$, 0.1, 0.3, and > 2 µm).
- *Experiment E2*: Toroidal magnetic field $B_t = 2.4$ T, plasma current $I_p = 1.0$ MA, core plasma density $n_e \sim 9.0 \times 10^{19}$ m^{-3}, and auxiliary heating $P_{ECRH} = 3.3$ MW. The electron temperature peaked at $T_e \sim 20$–30 eV, while the exposure time was cut to ~ 6 s. The ELM

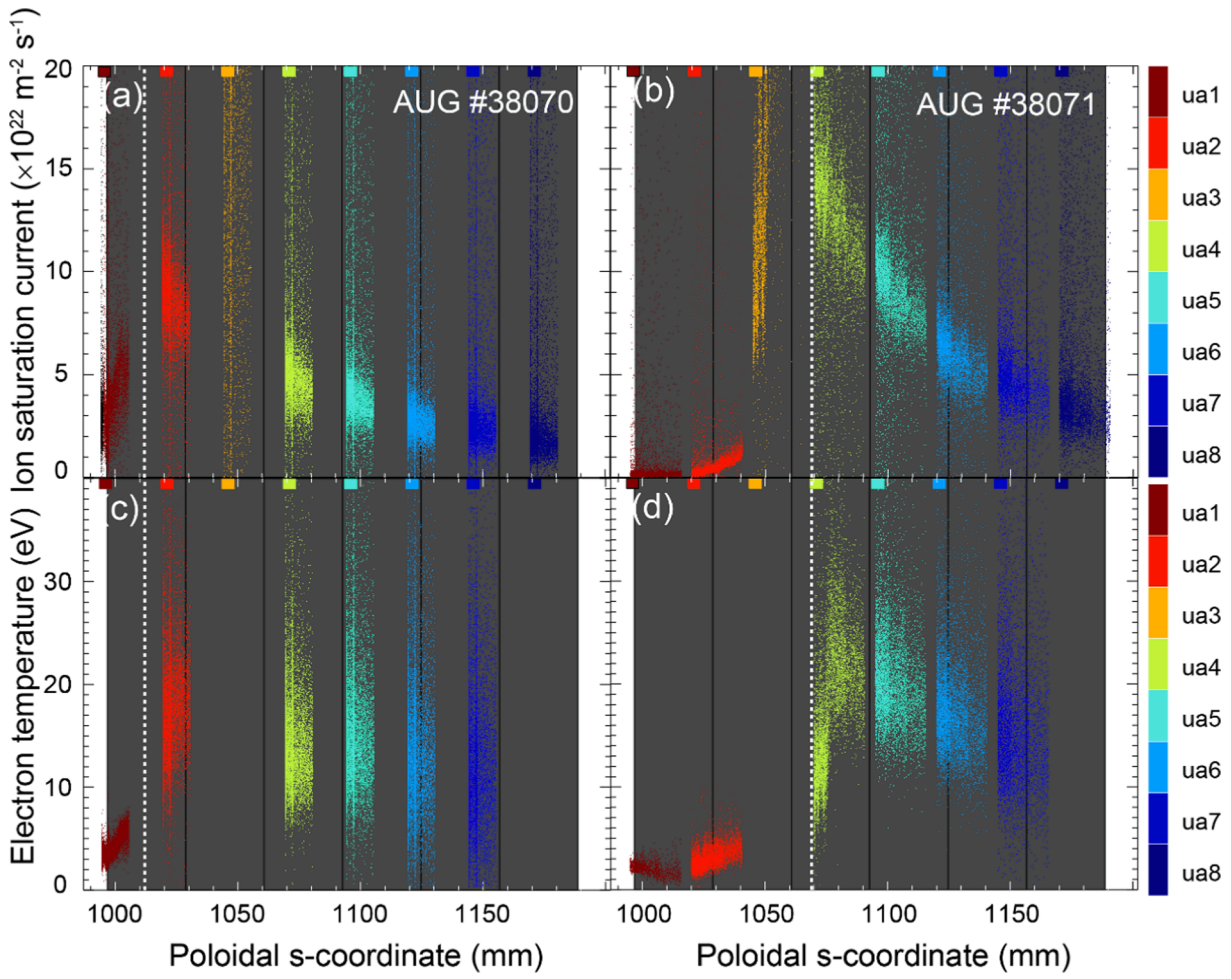

Fig. 3. (a, b) Ion saturation current at the divertor, measured using Langmuir probes (ua1-ua8), during (a) the OSP1 phase (discharge #38070) and (b) the OSP2 phase (discharge #38071). (c, d) corresponding profiles for the electron temperature. The grey bars denote the poloidal locations of the samples (according to Fig. 1) and the white dashed lines the locations of the strike points.

frequency and related energy loss were 50 Hz and 20 kJ, respectively, see [1] while the normalized ELM energy loss was estimated to $\Delta W_{ELM}/W_{MHD} \sim 0.043$. According to Fig. 1c, identical S-a samples to those in experiment E1b had been mounted on the DIM-II head, in addition to which a Mo-coated bulk W tile with a 30-mm wide Au stripe was used; this particular marker tile is not discussed here (see [1] for details).

Net erosion and deposition behaviour in H-mode plasmas

In the following we will discuss the net erosion/deposition results determined for the exposed type S-b Mo roughness samples as well as for the type S-a Au markers and discuss the deposition of W impurities on the roughness samples.

Erosion characteristics of Mo roughness samples

All the investigated type S-b roughness samples exhibited similar net-erosion behaviour in the poloidal direction and consistently indicated that an increased surface roughness will lead to reduced net-erosion rates. This can be seen in Fig. 5a where the erosion/deposition rates of the three different Mo marker coatings, determined using RBS, as a function of distance from OSP1 are shown; negative values for the distance correspond to the private flux region. One can also see that the erosion profiles are broad – the main peak around OSP1 spans a poloidal range of ~ 40–50 mm – in contrast to the L-mode case (see [1] and Fig. 5b) where net erosion is only measured within 10–15 mm from the strike point.

A comparison between the L- and H-mode roughness samples, also in terms of distance from the OSP, can be seen in Fig. 5b. From this, we conclude that the erosion rates in H-mode are 2–5 times larger than in L-mode and such that the erosion peak around the strike point for the smoothest L-mode sample ($R_a \sim 0.004$ μm) is comparable to the erosion rate determined for H-mode samples with some two orders of rougher surfaces ($R_a \sim 0.3$ μm). Data in [1] already indicated erosion to increase by a factor of 2 when switching from L- to H-mode and keeping the T_e and surface roughness unchanged, thus the H-mode data sets in Fig. 5b are to a large extent representative counterparts for those extracted from experiment E1b.

In the present experiment E3, net deposition is observed below OSP1 but also at elevated positive distances, beyond a distance of 25–35 mm. The latter can be explained by the uppermost parts of the roughness samples being located just below OSP2, strike point of the subsequent exposure phase (see Fig. 1a); Analyses in Ref. [17] hint that the extent of prominent deposition in the PFR can span across a poloidal distance of > 15–20 mm in a similar plasma scenario. The measured Mo inventories are therefore a combination of material transport from around OSP1 and OSP2; in both cases Mo is the main marker material. Despite these complexities in interpreting especially the occurrence of deposition peaks, one already notices from Fig. 5a that the rougher the sample, the earlier net erosion changes into net deposition and the thicker the deposits will become towards OSP2.

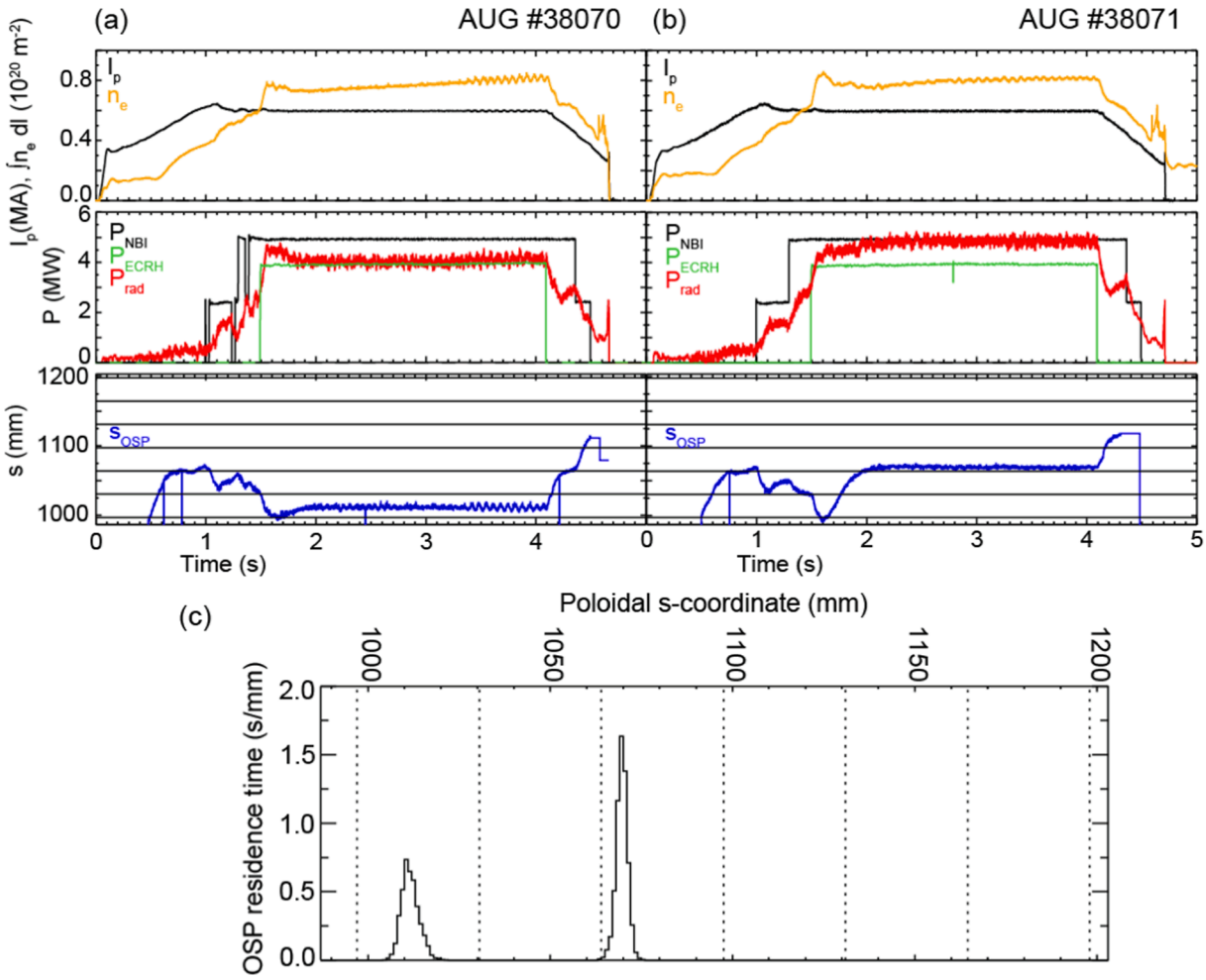

Fig. 4. (a, b) Examples of time traces of key plasma parameters during the present H-mode experiment E3 in (a) the OSP1 phase (AUG discharge #38070) and (b) the OSP2 phase (AUG discharge #38071). (c) Approximate residence time for the OSP as a function of the poloidal s-coordinate in the two phases of the experiment. The dotted lines indicate the start and end coordinates for the individual inserts (see Fig. 1). Please note that the residence time needs to be convolved with particle flux and ion energy to provide the OSP coordinates.

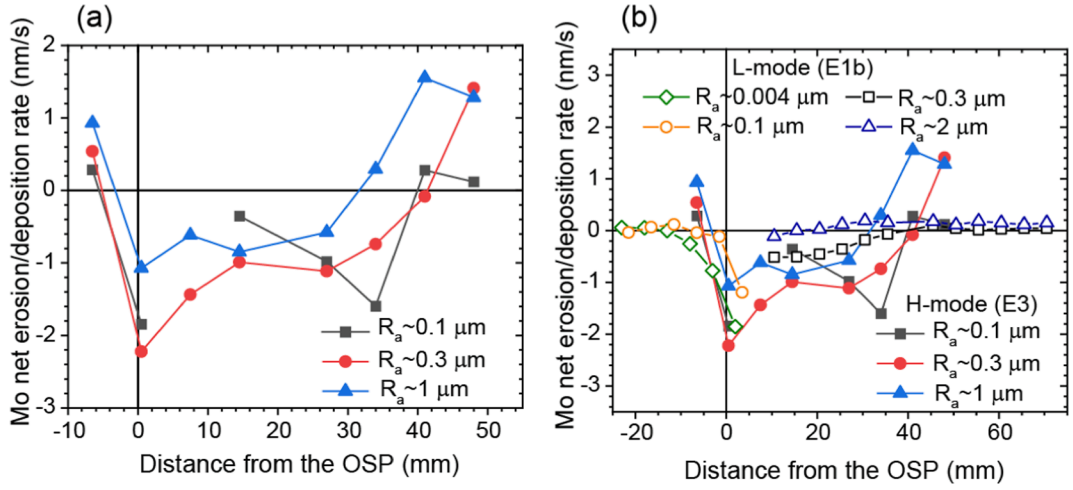

Fig. 5. Poloidal net erosion/deposition (negative/positive values) profiles for the different Mo roughness samples (type S-b) as a function of distance from the OSP (OSP1 in the case of experiment E3). In (a), the data from the present H-mode experiment E3 is shown and in (b) results from both experiment E3 and the L-mode experiment E1b are summarized. Negative values for the distance refer to the private flux region. In (a), the non-continuous profile for the $R_a \sim 0.1$ µm samples is due to missing data points around the strike point. The error bars due to the RBS procedure are ~ 10 %.

A remaining puzzling observation is connected with the net-erosion behaviour of the smoothest studied samples ($R_a \sim 0.1$ μm): net erosion shows a distinct peak around OSP1 but is then strongly reduced towards higher values of the s-coordinate. Only further away the situation slowly returns to what would have been expected from the surface roughness only, i.e., the smoothest samples are eroded the most and show the thinnest deposits [1]. The reason for these trends can be speculated to result from deposition of material from the neighbouring set of marker samples, the ones with the nominal roughness of $R_a \sim 0.3$ μm, located toroidally upstream of the smoothest ones (see Fig. 1a). According to [1], in H-mode material can migrate at distances several cm from their origin, so a fraction of particles originating from the "leftmost" sample can end up on the surface of the "rightmost" sample on the same target tile.

Another factor that may have contributed to the shapes of the profiles in Fig. 5a is related to the post-exposure measurements made spatially twice as frequently as the pre-exposure ones. Thus extrapolations were mandatory to obtain estimates for the erosion rates and here even a small uncertainty of 1–2 % in the original thickness of the markers (2–3 nm vs 150 nm) in between two pre-exposure measurement points could result in up to ~ 20 % error in the determined erosion rates. This exceeds the typical uncertainties of up to 10 % related to RBS, mainly due to inaccuracies in beam-current measurements.

In the deposition-dominated private flux region, approximately-three times more material is accumulated on the roughest samples than on the smoother ones. A comparable behaviour was observed in [1], where also deposition of different impurities on W marker coatings was investigated in L-mode.

Erosion of Au marker samples

The exposed gold marker samples showed uniform and strong net erosion throughout the entire analyzed region. This can be best noticed in Fig. 6a where the determined net-erosion profiles of both the 1 × 1 mm^2 and 5 × 5 mm^2 marker spots (extracted from micro-PIXE and broad-beam RBS measurements, respectively) are shown as a function of poloidal distance from OSP2. The main erosion peak takes place close to OSP2, within a poloidal range of 30–40 mm, quite consistently with the results extracted from the Mo roughness samples in Section 3.1. Net erosion appears to saturate to a level of ~ 2.5–4 nm/s in the peripheral region unlike what has been, e.g., determined after experiment E1b: erosion almost completely vanishes, even turns into marginal but measurable net deposition, at distances beyond ~ 40–50 mm from the strike point [10]. On the other hand, similarly constant and strong erosion rates have been measured for Mo markers following their exposure to helium plasmas on AUG, as reported in [1].

Comparison between the two different marker spots reveals that the smaller ones (1 × 1 mm^2) are more strongly eroded than the larger ones (5 × 5 mm^2): up to 6 nm/s vs about 5 nm/s around OSP2. This agrees with the published results from the L- and H-mode experiments (see [1,10]): in L-mode the small markers exhibited 10–20 % higher erosion rates than the larger ones, whereas in H-mode erosion was amplified by a factor of 1.5–2 for the small marker spots. Here the ratio of "only" 1.2–1.3 can be associated with the 1 × 1 mm^2 spots being badly damaged after the experiment such that little of the original coating was left on the surface. The erosion rates in Fig. 6a may thus be underestimations of the actual situation. Similarly to the discussion in [10], net erosion and the accompanying re-deposition are efficiently caught by the analyses of the large marker spots while the smaller marker spots can be used for gross-erosion investigations, with the caveat that re-deposition on them can still be substantial at the present plasma conditions [18].

The considerable net erosion throughout the entire analysed poloidal region and complete lack of net deposition is qualitatively different from what has been determined for the Mo roughness samples in Fig. 5. Here we need to keep in mind that even though the plasma flux peaked close to the strike point, all the samples even at a distance of several cm from it saw some part of the flux, thus the overall exposure time on the Au marker spots had been higher than the 9 s attributed to the OSP2 phase. In the extreme case, if the markers had been subjected to the same high flux during the entire 15 s of experiment E3 (OSP1 + OSP2 phases), the erosion rates would have dropped to ~ 3 nm/s close to the strike point and ~ 1.5 nm/s in the far scrape-off layer. These actually correspond well to what has been previously evaluated either for the Mo roughness samples or the samples from previous L- and H-mode experiments (in [1]). Nevertheless, due to the lower plasma flux on the Au markers during the OSP1 phase than in the subsequent OSP2 phase (see Fig. 3), the erosion rates are expected to be closer to the maximum values obtained from Fig. 6a and stated above.

Fig. 6b shows the erosion profiles for the 5 × 5 mm^2 marker spots from experiment E3 together with the available data from experiments E1b and E2. The estimated erosion rates in experiment E3 are a factor of 5 higher than in L-mode and 2–3 times larger than in experiment E2. Besides the possible overestimation of the erosion rates as discussed in

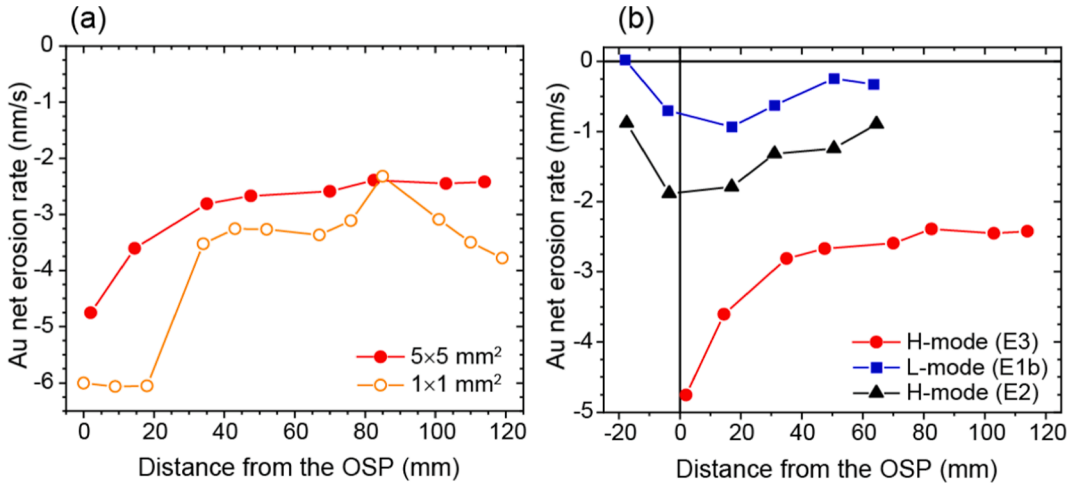

Fig. 6. Poloidal net erosion profiles (a) for the 5 × 5 mm^2 and 1 × 1 mm^2 Au marker spots (type S-a) following experiment E3 and (b) for the 5 × 5 mm^2 Au marker spots during experiments E1b (L-mode), E2 (H-mode), and E3 (H-mode), in both cases as a function of distance from the OSP (OSP2 in the case of experiment E3). Negative values for the distance refer to the private flux region. Note that in (a) the erosion rates for the 1 × 1 mm^2 spots in the region 0–20 mm can be underestimations of the actual situation due to almost complete erosion of the markers. The error bars due to the RBS procedure are ~ 10 %. For the 1 × 1 mm^2 Au markers the lack of pre-exposure measurements increases the error to ~ 20 %.

the previous paragraph, the smoother surface of the Au markers (R_a < 0.2 μm vs R_a ~ 1 μm) has clearly contributed to the balance between erosion and re-deposition: according to [1] (see Figs. 5 and 7 therein), a factor of 5–10 change is expected, when the roughness changes by an order of magnitude.

Deposition of W on roughness samples

Deposition of impurities was inspected by measuring the accumulation of W on the exposed Mo and Au marker samples from other areas of the AUG torus, either from the divertor or from the main chamber. Light impurities, most notably boron (B) from regular boronizations of the AUG vessel, are not discussed here but will the subject of future studies. In the case of gold, interpretations were somewhat complicated by the Au and W signals interfering with each other or the related measurement peaks partially overlapping, almost independent of the applied analysis technique (RBS, PIXE, or SEM-EDX). However, for the samples studied here this mainly resulted in error bars becoming larger than typically is the case for deposition investigations (~20 % instead of ~ 10 %). Nevertheless, in the following we will exclusively analyse the different Mo roughness samples.

Fig. 7a shows the poloidal W deposition profiles for the different Mo roughness samples, measured using broad-beam RBS, together with corresponding poloidal profiles for the W/Mo ratio, extracted from the available SEM-EDX data (taken with the electron beam energy of 5 keV). Both RBS and SEM-EDX demonstrate deposition to enhance with increasing distance from the strike point (OSP1) and peak in the region where net deposition for Mo was apparent (see Fig. 5a, below OSP2). However, no obvious trends with respect to the surface roughness can be identified between the two methods. On the roughest samples (R_a ~ 1 μm), deposition remains at a surprisingly low level, while based on [1] one would have expected these samples to show the most prominent layers. The other two samples are more in line with the prediction by the surface-roughness hypothesis.

As mentioned above, the deposition profiles for light impurities are not yet available but the details of the measured RBS spectra already indicate deposition of, e.g., carbon and boron to be the strongest on the roughest samples. This apparent contradiction will be addressed in a future publication but it could be connected with the microscopic surface structure as will be discussed below. The microstructure can also clarify why broad-beam RBS shows deposition to increase the deeper into the private flux region layer one proceeds while SEM-EDX does not give any hints on such behaviour, of course with the disclaimer that the SEM-EDX data below OSP1 is scarce.

The observations shown above can be better put into perspective with the help of the 2D elemental EDX maps from the different sample types, collected in Fig. 7b-d at a distance of ~ 23 mm from the strike point. While deposits on the plasma-etched samples (R_a ~ 0.1 μm and R_a ~ 0.3 μm) are relatively uniformly distributed throughout the surface and much more noticeable on the rougher one (see Fig. 7c, in terms of the amount of W), the layers on the glass-blasted samples (Fig. 7d) are inhomogeneous and qualitatively completely different from those on the other sample types. In particular, the "red" W signal is concentrated in areas with the size of a few dozens of micrometres and in between them extended "blue" regions denoting the presence of carbon appear. Carbon may result from deposition of light impurities during the plasmas or from holes in the original Mo coating. The extracted SEM images, however, do not clearly support any of the two hypotheses but in any case local non-uniformities may well explain why Fig. 7a suggests little deposition: the broad-beam RBS data is averaged over a mm^2-sized area

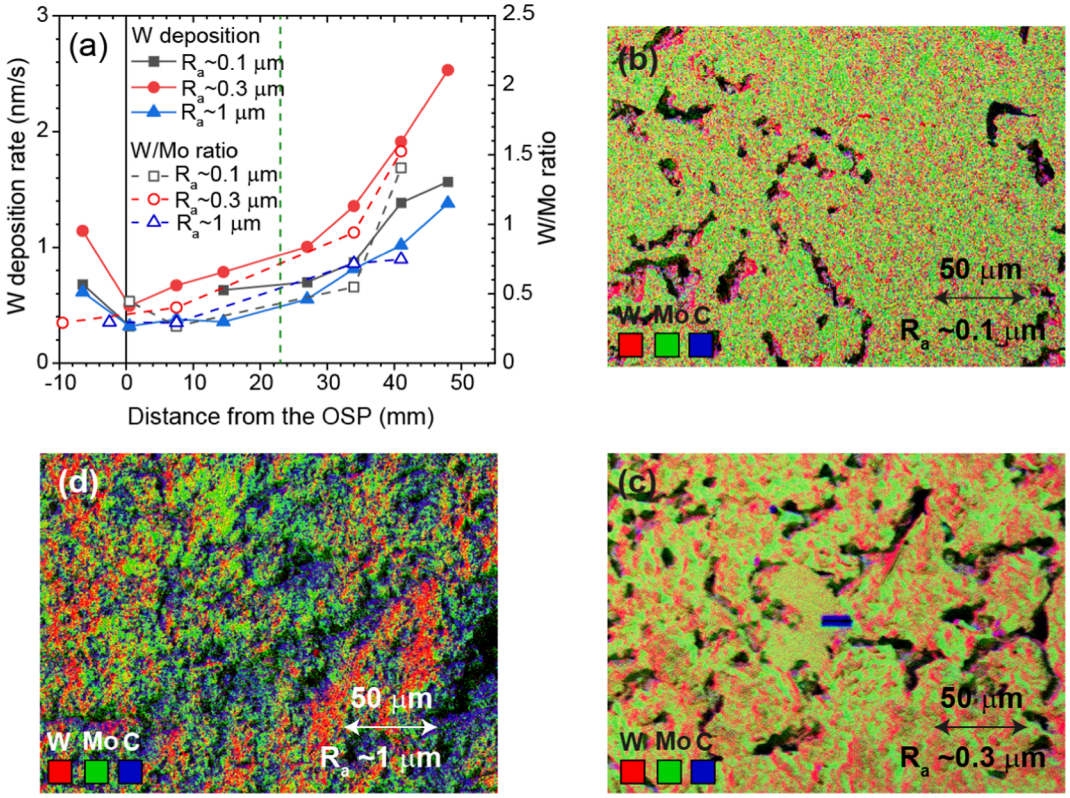

Fig. 7. (a) Poloidal deposition profiles of W (solid symbols and lines), measured using broad-beam RBS, together with the W/Mo intensity ratio (open symbols, dashed lines), determined by applying SEM-EDX with the electron beam energy of 5 keV, of the Mo roughness samples (type S-b) as a function of distance from OSP1. (b-d) EDX images of the 2D elemental maps of W (red), Mo (green), and carbon (blue) on (b) the R_a ~ 0.1 μm, (c) R_a ~ 0.3 μm, and (d) R_a ~ 1 μm sample at a distance of + 23 mm from OSP1 (denoted by a green dashed line in (a)). Note the rectangular feature at the centre of the EDX map in (c), where the carbon signal (blue) results from a focused ion beam cut through the layers down to the graphite substrate. (For interpretation of the references to colour in this figure legend, the reader is referred to the web version of this article.)

while the W/Mo ratio spanned over an area of $\sim 0.075 \times 0.1$ mm^2.

The conclusions are not altered for other values of the poloidal coordinate – only the deposits become more and more prominent the further one moves away from OSP1. Around OSP1, the surface of the plasma-etched samples becomes also more modified and/or damaged and there are large regions with W and metallic impurities impinged on them. All this gives additional proof that deposition follows the surface topography and simple determination of the amount of deposited material by averaged approaches cannot fully characterize deposition or erosion behaviour of plasma-facing surfaces. Furthermore, deposition in deeply recessed areas can be considered as an archaeological exercise where layered structures are expected to form and reflect the complex exposure history of the PFCs unlike less modified surfaces where deposits are continuously modified during the course of their plasma exposure.

Discussion and conclusions

We have investigated erosion and deposition characteristics of plasma-facing materials at the outer strike-point region of the AUG divertor during H-mode discharges with small and relatively frequent ELMs. Samples with pre-determined Mo or Au marker coatings and with different surface morphologies and geometries were inserted into the divertor plasma using the DIM-II manipulator, and changes in the thickness and composition of the surface layers were determined.

The obtained results were compared to the existing data from previous L- and H-mode experiments on AUG. Despite the different applied scenarios, the (inter-ELM) peak value for the electron temperature at the strike point was kept constant in all these experiments (around 20–30 eV) to result in measurable net erosion even during a short exposure period. Moreover, the present and the earlier H-mode experiment showed similar plasma fluxes in terms of the measured ion saturation current while the ELM sizes and frequencies varied from one experiment to another.

The results clearly showed that, analogously to the conclusions made for L-mode exposures, increasing surface roughness leads to reduced net erosion even though the effect in H-mode is not that prominent as the data from the analysed Mo roughness samples proves. Comparison between the two analysed H-mode experiments indicated that samples with a relatively smooth surface ($R_a < 0.2$ μm) may, on average, erode 2–3 times faster than the ones with a much rougher surface ($R_a \sim 1$ μm). However, here one should note that both the sequence of discharges applied on the samples as well as the details in the preparation of the markers were different.

We also noticed that in H-mode clearly distinguishable and prominent fluctuations can be seen in the poloidal and toroidal net-erosion and -deposition profiles. This can be connected with a large migration length of the eroded material, of the order of several cm, resulting in strong competition between erosion and re-deposition especially at distances > 50 mm away from the strike point; in this region, and in the geometry of the present experiment E3, the $\mathbf{E} \times \mathbf{B}$ drift tends to drive particles poloidally outwards away from the vicinity of the strike point but the electron temperature and plasma flux are still high enough to result in measurable sputtering, see [16] for details. It is, however, worth noticing that migration especially in the toroidal direction is a hypothesis and up to now is not directly supported experimentally due to the issues in reaching high enough signal-to-noise ratios for measurements outside of the gold marker spots. In addition, due to the short duration of the experiment even small uncertainties in the original thickness of the coating can lead to > 20 % error bars in the determined erosion rates. In general, net-erosion rates were 2–5 times higher in H-mode than in L-mode and also the deposition in the private flux region was more noticeable in the H-mode case, though the database in the private flux region is relatively limited.

Understanding deposition of various impurities, both heavy (like W) and light ones, on PFCs requires careful analyses in the microscopic scale. Generally, deposition is enhanced the rougher the sample surface becomes which is most clearly seen for light impurities. However, the roughest surfaces also showed lots of non-uniformities on their marker coatings, even the integrity of the produced layers was compromised, thus resulting in the appearance of a complex pattern of peaks and shadowed areas on the surfaces in the micrometre scale. Accumulation of material is strong at the bottom of the "valleys" but these deposition-rich areas tend to average out when considering a large enough region where also damaged areas of the original coating are included. On the other hand, noticeable deposition of W on the most eroded samples is consistent with the fact that the impinging plasma flux brings along W from neighbouring areas or even from different parts of the vessel, including the main chamber as discussed in [16].

The strong and persistent erosion throughout the exposed Au marker samples could be attributed, besides their surface roughness, to the samples being subjected to the (peripheral) plasmas during both phases of the studied H-mode experiment: the tails of the plasma flux and electron-temperature profiles in the common SOL were still considerable at distances > 50 mm from the strike point, of the same order of magnitude as what has been measured for the L-mode case at the OSP. This may also provide an explanation to observations in helium plasmas in [1] where a similar split of the actual experiment in two phases was implemented.

The main conclusions are that local plasma parameters have a huge impact on PFC erosion rates and, besides of incident plasma flux, surface morphology and its temporal evolution have to be taken into account for quantitative estimates of erosion rates and PFC lifetime under reactor-relevant conditions.

CRediT authorship contribution statement

A. Lahtinen: Formal analysis, Investigation, Writing – original draft. **A. Hakola:** Conceptualization, Methodology, Formal analysis, Writing – review & editing. **J. Likonen:** Conceptualization, Validation. **M. Balden:** Investigation, Resources, Writing – review & editing. **K. Krieger:** Conceptualization, Investigation, Resources. **S. Gouasmia:** Investigation. **I. Bogdanovic Radovic:** Investigation, Resources. **G. Provatas:** Investigation. **M. Kelemen:** Investigation. **S. Markelj:** Resources. **M. Pedroni:** Investigation. **A. Uccello:** Resources. **E. Vassallo:** Investigation. **D. Dellasega:** Investigation. **M. Passoni:** Resources.

Declaration of Competing Interest

The authors declare the following financial interests/personal relationships which may be considered as potential competing interests: [Antti Hakola reports financial support was provided by EUROfusion.].

Data availability

Data will be made available on request.

Acknowledgments

This work has been carried out within the framework of the EUROfusion Consortium, funded by the European Union via the Euratom Research and Training Programme (Grant Agreement No 101052200 — EUROfusion). Views and opinions expressed are however those of the author(s) only and do not necessarily reflect those of the European Union or the European Commission. Neither the European Union nor the European Commission can be held responsible for them. Part of the work performed under EUROfusion WP PWIE.

Antti Hakola reports financial support was provided by EUROfusion.

Appendix A. Supplementary material

Supplementary data to this article can be found online at https://doi.

org/10.1016/j.nme.2022.101266.

References

[1] A. Hakola, et al., Nucl. Fusion 61 (2021), 116006.
[2] J. Guterl, et al., Plasma Phys. Control. Fusion 61 (2019), 125015.
[3] D.L. Rudakov, et al., Phys. Scr. T159 (2014), 014030.
[4] S. Brezinsek, et al., Nucl. Fusion 59 (2019), 096035.
[5] M. Balden, et al., Phys. Scr. 96 (2021), 124020.
[6] K. Schmid, et al., Nucl. Fusion 50 (2010), 105004.
[7] M. Mayer, et al., Phys. Scr. T128 (2007) 106.
[8] M. Mayer, et al., Phys. Scr. T171 (2020), 014035.
[9] K. Krieger, et al., Phys. Scr. T171 (2020), 014037.
[10] A. Hakola, et al., Nucl. Mater. Energy 25 (2020), 100863.
[11] A. Lahtinen, et al., Europhysics Conf. Abstracts 41F (2017) P2.119.
[12] A. Herrmann, et al., Fusion Eng. Des. 98–99 (2015) 1496.
[13] S. Lehto, et al., Fusion Eng. Des. 66–68 (2003) 241.
[14] M. Mayer, Report **IPP 9/113** (1997) SIMNRA User's Guide.
[15] A. Hakola, et al., Nucl. Fusion 57 (2017), 086019.
[16] A. Hakola, et al., Nucl. Mater. Energy 12 (2017) 423.
[17] K. Krieger et al., Boron redistribution after boron powder injection in ASDEX Upgrade, this conference.
[18] R. Ding, et al., Nucl. Fusion 56 (2016), 016021.